

Adaptive multiscale reconstruction of buried objects

Alexandre Baussard^{1,3}, Eric L Miller² and Dominique Lesselier¹

¹ Département de Recherche en Électromagnétisme, Laboratoire des Signaux et Systèmes (CNRS/SUPELEC/UPS), 3 rue Joliot-Curie, 91192 Gif-sur-Yvette, France

² Center for Subsurface Sensing and Imaging Systems, Northeastern University, 315 Stearns Hall, Boston, MA 02115-5000, USA

E-mail: alexandre.baussard@ensieta.fr

Received 25 March 2004, in final form 20 September 2004

Published 8 November 2004

Online at stacks.iop.org/IP/20/S1

doi:10.1088/0266-5611/20/6/S01

Abstract

In this contribution, an adaptive multiscale approach for the localization and characterization of buried objects in a half-space is proposed. The main goal of the approach is to reduce the number of elements to be estimated and so the degrees of freedom in the unknown profile. This leads to improvement of the robustness of the inversion and to an increase in the quality of reconstruction. The proposed inversion scheme is based on an adaptive, coarse-to-fine iterative strategy using spline pyramids. The global procedure consists of sequences of non-linear inversions separated by refinement steps, which overall produces an accurate, low-order representation of the sought object.

1. Introduction

The detection and characterization of objects buried in a half-space from measurements of the scattered response of a known electromagnetic excitation arise in various applications such as Earth subsurface sensing, humanitarian demining, medical imaging and nondestructive testing. In this paper, the general problem of the non-linearized reconstruction of two-dimensional subsurface heterogeneities is considered. The goal is to retrieve constitutive parameters of buried objects (geometry, electrical characteristics) from time-harmonic wave field data collected above the half-space. This is a challenging problem, in particular due to the severe ill-posedness which is caused by the availability of aspect-limited data only.

Many algorithms have already been developed to solve this kind of inverse scattering problem, such as those in [3, 6, 9, 10, 15]. Typically, these methods solve a large-scale, non-linear optimization problem by generating values for every pixel covering the test area, including those which might not contain any useful information about the objects.

In previous work [1, 2], in order to reduce the number of unknowns to be estimated, an adaptive B-spline scheme was proposed. The test domain was represented by a spline surface parametrized by a knot distribution [5] adaptively determined during the process.

³ Present address: E3I2-ENSIETA, 2 rue François Verny, 29806 Brest, France.

In the present contribution, starting from this previous work and inspired also by an earlier solution of a one-dimensional inverse scattering problem for a diffusion coefficient [11], an adaptive multiscale approach based on spline pyramids [14] is proposed. This multiscale representation of the unknown parameters enables a low-order reconstruction for which the distribution of fine-scale detail is determined via an automatic refinement procedure. That is, starting with a coarse-scale set of spline functions, the sought distribution is iteratively refined by introducing finer-scale spline functions in ‘areas of interest’ (say, where objects are emerging from the background); then, the final estimate consists of functions at several scales.

The general idea and resulting scheme of the proposed adaptive multiscale approach take a substantial departure from the adaptive B-spline approach proposed in [2]. In this previous work, the object was represented by means of a B-spline basis in which one set of knots was defined along the x -axis and another one along the y -axis. The influence of the locations of these knots was somewhat ‘global’ in that, e.g., a change in the location of an x -axis knot generally impacted the structure of the object in a vertical region covering the whole y -axis. Using B-splines in this manner led to the presence of artifacts in images when there were multiple objects in the domain of interest. In this contribution, the newly proposed representation, based on spline pyramids, leads to a more ‘local’ description by which it is meant that each basis permits us to individually ‘describe’ a part of the image and enables better reconstructions.

Moreover, the presently proposed adaptive ‘coarse-to-fine’ procedure imposes smoothness conditions at coarse resolutions, which tends to regularize the inversion problem; there is no need for explicit regularization using, e.g., a Tikhonov-type functional (which would involve us setting a proper weighting parameter).

The paper is organized as follows. In section 2 the formulation of the problem is introduced. In section 3 the proposed adaptive multiscale algorithm is described. In section 4, numerical results obtained using the proposed scheme and a standard one (pixel-based conjugate-gradient inversion scheme) are shown. In section 5 concluding remarks are made.

2. Problem statement

The geometry of the problem studied is depicted in figure 1 where two homogeneous half-spaces (numbered 1 and 2) are separated by a planar interface. Possibly inhomogeneous, penetrable cylindrical obstacles (Ω) with z -axis are fully embedded in half-space 2, inside a prescribed domain \mathcal{D} .

All constitutive materials are assumed linear, isotropic and non-magnetic. Their permittivities read as $\varepsilon_m = \varepsilon_0 \varepsilon_{rm}$, $m = 1, 2, \Omega$, at implied circular frequency ω —omitting the time-dependence $\exp(-i\omega t)$ —where ε_0 is the permittivity of half-space 1 (henceforth assumed to be air), and where both ε_{r2} and $\varepsilon_{r\Omega}$ might take frequency-dependent, complex values. The corresponding propagation constants k_m are defined as $k_m^2 = \omega^2 \mu_0 \varepsilon_m$.

Ideal time-harmonic electric current line sources S_l ($l = 1, \dots, N_s$), set parallel to the z -axis (transverse magnetic (TM) polarized), are equally distributed above the interface at constant height y_s . Similarly ideal sensors are also equally distributed above the interface at constant height y_r (domain Γ) and collect the single z -component of the scattered electrical field e^d at N_r locations.

Starting from the Maxwell equations and using the Green theorem, the forward scattering problem is formulated via the usual domain integral equations:

$$e(\mathbf{r}) = e^{inc}(\mathbf{r}) + \int_{\mathcal{D}} \chi(\mathbf{r}') G_{22}(\mathbf{r}, \mathbf{r}') e(\mathbf{r}') d\mathbf{r}', \quad \mathbf{r} \in \mathcal{D}, \quad (1)$$

$$e^d(\mathbf{r}) = \int_{\mathcal{D}} \chi(\mathbf{r}') G_{12}(\mathbf{r}, \mathbf{r}') e(\mathbf{r}') d\mathbf{r}', \quad \mathbf{r} \in \Gamma, \quad (2)$$

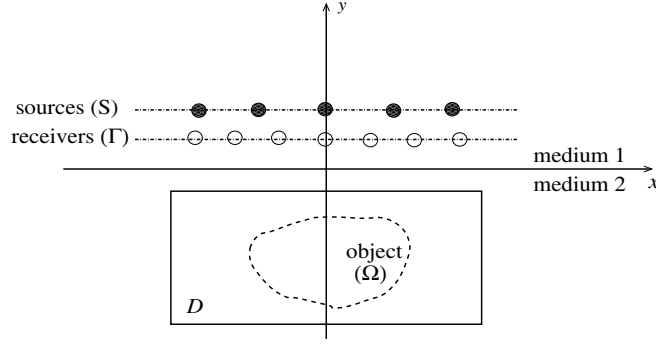


Figure 1. Geometrical configuration of study.

where $\chi(\mathbf{r}) = \varepsilon_{r\Omega}(\mathbf{r}) - \varepsilon_{r2}$ is the contrast function defined in \mathcal{D} , and e and e^{inc} are the single z -components of the total field and of the incident field, respectively. $G_{mn}(\mathbf{r}, \mathbf{r}')$ are the Green functions which model the radiation of a Dirac-type source at \mathbf{r}' in the half-space n and the observation of the field at \mathbf{r} in the half-space m .

By discretizing the search domain into a regular mesh (N_x cells along the x -axis and N_y cells along the y -axis) and using a standard pulse-basis point-matching method of moments [8], state equation (1) and observation equation (2) can be written, for each illumination l ($l = 1, \dots, N_s$), as matrix equations

$$\mathbf{e}_l = \mathbf{e}_l^{inc} + \mathbf{G}_{22}D(\mathbf{c})\mathbf{e}_l, \quad (3)$$

$$\mathbf{e}_l^d = \mathbf{G}_{12}D(\mathbf{c})\mathbf{e}_l, \quad (4)$$

where \mathbf{e}_l is the total field vector and \mathbf{e}_l^{inc} is the incident field vector, both of dimension $N (= N_x \times N_y)$, \mathbf{e}_l^d is the scattered field vector of dimension N_r , and \mathbf{G}_{22} and \mathbf{G}_{12} are $[N \times N]$ and $[N_r \times N]$ matrices made of properly integrated Green functions [7, 8]. $D(\mathbf{c})$ is a $[N \times N]$ diagonal matrix whose entries are the elements of the N -sized contrast vector \mathbf{c} .

These two equations can be expressed as a unique non-linear equation in \mathbf{c} :

$$\mathbf{e}_l^d = \mathbf{G}_{12}D(\mathbf{c})[\mathbf{I}_d - \mathbf{G}_{22}D(\mathbf{c})]^{-1}\mathbf{e}_l^{inc}, \quad (5)$$

where \mathbf{I}_d denotes the identity matrix of dimension $[N \times N]$.

3. Adaptive multiscale approach

3.1. An overview of spline pyramids

Splines are piecewise polynomials the pieces of which are smoothly connected together. They can be uniquely characterized in terms of a B-spline expansion as

$$s(x, y) = \sum_{k \in \mathbb{Z}} \sum_{l \in \mathbb{Z}} a(k, l) \beta^m(x - k) \beta^m(y - l), \quad (6)$$

which involves integral shifts of the central B-spline of degree m denoted as $\beta^m(x)$. The parameters of the model are the B-spline coefficients $a(k, l)$. B-splines are symmetrical,

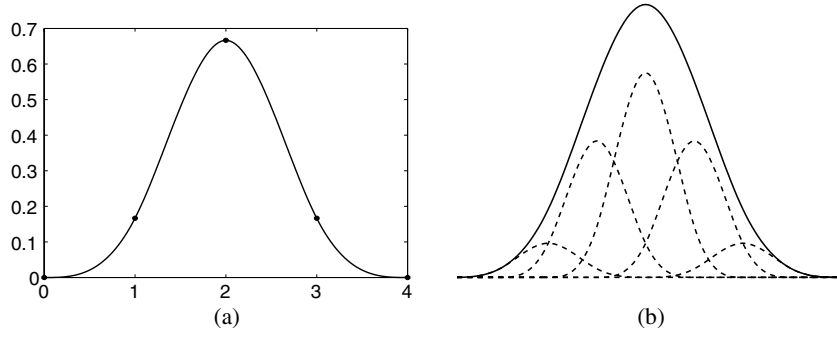


Figure 2. (a) One-dimensional cubic B-spline (scale 0, i.e., finer scale). (b) two-scale relation for the cubic B-spline: scale s (—) and scale $s - 1$ (- - -).

bell-shaped functions constructed from an $(m + 1)$ -fold convolution of a rectangular pulse $\beta^0(x)$:

$$\beta^m(x) = \underbrace{(\beta^0 * \beta^0 * \dots * \beta^0)}_{(m+1) \text{ times}}(x) \quad \text{with } \beta^0(x) = \begin{cases} 1 & \text{if } -\frac{1}{2} < x < \frac{1}{2}, \\ \frac{1}{2} & \text{if } |x| = \frac{1}{2}, \\ 0 & \text{otherwise.} \end{cases} \quad (7)$$

Within the area of multiscale signal and image processing, B-splines have proven quite useful because they possess a convenient ‘nesting’ property. That is, a B-spline may be written as a linear superposition of dilated and translated versions of itself. More formally, one has a two-scale dilation equation of the form [12]

$$\beta(x) = \sum_{k=0}^{N_k-1} \alpha_k \beta(2x - k) \quad (8)$$

thereby making B-splines well suited for the synthesis of multiscale processing methods. α_k are the expansion coefficients. In figure 2(b), an illustration of the two-scale relation for a B-spline of degree 3 (figure 2(a)) is exemplified.

Spline pyramids provide a very convenient tool for performing multiscale image processing. In [11], the two-scale relationship was exploited in the development of a one-dimensional non-linear inversion method in which details were iteratively added and pruned from an underlying representation of the unknown object. The resulting technique provided for an adaptively determined, parsimonious representation of the object in which fine-scale details were ‘automatically’ put in the proper areas. Moreover, iterative algorithms based on a multiscale approach tend to be less likely to get trapped in a local optimum, as shown in an image registration algorithm [13, 14].

3.2. Adaptive multiscale algorithm

The solution of the inverse problem consists of building up a map of the distribution of the constitutive parameters (permittivity and/or conductivity) throughout the search domain, from the scattered field data. In this contribution, an adaptive multiscale scheme based on the previous spline pyramids is proposed, which leads us to ‘describe’ the unknown parameters via spline functions at several scales. The distribution should be as follows: fine-scale functions in areas where there are significant details such as edges or textured regions, and coarse-scale

functions elsewhere. The key point is that this distribution is determined automatically by the algorithm with no *a priori* information about the parameters. The contrast function is defined as

$$\mathbf{c} = \mathbf{B}\mathbf{a}, \quad (9)$$

where \mathbf{a} is the expansion coefficient vector of dimension $N_a \ll N$ and \mathbf{B} is the $[N \times N_a]$ matrix, the columns of which correspond to tensor products of B-spline functions. As basis functions, the popular cubic B-splines (see figure 2(a)) are considered for their useful properties of data fitting and smoothness [14].

From (5) and taking into account (9), the inverse problem is solved by minimizing the cost functional:

$$J(\mathbf{a}) = W \sum_{l=1}^{N_s} \|\mathbf{e}_l^d - \mathbf{G}_{12}D(\mathbf{B}\mathbf{a})(\mathbf{I}_d - \mathbf{G}_{22}D(\mathbf{B}\mathbf{a}))^{-1}\mathbf{e}_l^{inc}\|^2, \quad (10)$$

where W is a normalizing coefficient defined as

$$W = \frac{1}{\sum_{l=1}^{N_s} \|\mathbf{e}_l^d\|^2} \quad (11)$$

which is introduced in order to have normalized evolutions of the cost functional values and to facilitate numerical comparisons (this coefficient does not influence the convergence of the cost function). Minimization of (10) is performed in standard fashion via a conjugate-gradient algorithm [2, 6].

The global algorithm takes advantage of the iterative nature of the minimization procedure by adapting the local resolution of the object between sequences of iterations. This adaptive multiscale algorithm, which is a coarse-to-fine procedure, can be described as follows:

S1: From a coarse collection of cubic B-splines (e.g., figure 3(b)), minimize (10).

S2: Iterative procedure

S2.1: Refine the representation by introducing a finer-scale representation in ‘areas of interest’ (i.e., obstacles emerging in the search domain).

S2.2: Minimize (10), using as initial guess the previous object estimation.

S2.3: Go back to S2.1 until the representation cannot be refined anymore, until the minimal criterion value is reached, or until the maximum number of iterations is reached (the number of iterations in the minimization steps S1 and S2.2 and the number of iterations of stage S2 can be fixed at the beginning of the procedure).

Roughly speaking, the goal of refinement stage S2.1 is to replace a coarse-scale B-spline by its finer-scale representation only within those areas where it appears interesting to get a more detailed representation. Determining which basis functions to refine is accomplished as follows: one replaces a B-spline by its finer representation, and one subsequently attempts to estimate whether or not this new representation has any positive influence on the image reconstruction, i.e., for us, on the value of the cost functional. Since this approach requires the solution of a non-linear optimization problem, it might unduly increase the computational burden of the global procedure. So, in order to avoid this situation, the total field is kept constant during S2.1. One expects that this ‘linearization’ does not influence directly the reconstruction since one just investigates whether or not a more detailed representation of local parts of the image might be needed.

Steps taken at stage S2.1 can be summarized as follows:

S2.1.1: Compute a so-called reference cost value J'_{ref} by minimizing

$$J'(\mathbf{a}) = W \sum_{l=1}^{N_s} \|\rho'_l(\mathbf{a})\|^2, \quad (12)$$

where $\rho'_l(\mathbf{a}) = \mathbf{e}_l^d - \mathbf{G}_{12}D(\mathbf{B}\mathbf{a})\mathbf{e}_l$.

S2.1.2: Iterate the following steps:

- replace the i th ($i = 1, \dots, N_a$) B-spline (at scale s , if $s > 0$) by its finer-scale B-splines (i.e., basis at scale $s - 1$),
- from equation (12), compute the corresponding cost value J'_i ,
- put back the i th B-spline.

S2.1.3: Replace the B-splines in \mathbf{B} by their finer-scale counterparts only if this influences the reconstruction in a ‘good’ fashion, i.e., if the cost values calculated above satisfy the following criterion:

$$\frac{J'_{ref} - J'_i}{\max_{i=1, \dots, N_a} (J'_{ref} - J'_i)} > Th, \quad (13)$$

where Th is a threshold to be fixed ($Th \in [01]$).

In stage S2, one also considers that, if it is not possible to refine a B-spline function at a given scale over three successive iterations, one keeps this function (i.e., one does not try again to refine it).

In this contribution, the considered refinement scheme is based on a ‘one-by-one’ basis test, that is, only one B-spline is refined at each test, all others being kept the same. Then, B-splines which meet the criterion are replaced in step S2.1.3. This can be seen as an approximation of a more general scheme where all combinations of refinements would be tested in order to determine the best one. Although optimal, this combinatorial approach to the problem is generally rather intractable. Thus, motivated by similar work in the area of adaptive basis selection using greedy type methods [4], here one uses the ‘one-by-one’ procedure to evaluate the utility of refining a basis function.

Also, one considers that the criterion chosen in order to refine the spline representation (equation (13)) enables us to introduce finer-scale functions efficiently (i.e., within the objects and their neighbourhoods). One does not test whether or not it is interesting to replace finer scales by coarser ones in the representation, avoiding in particular a considerable increase in computational time. Let us notice that this is in contrast with previous contribution [11].

Finally, the estimated object is composed of functions at several scales (e.g., figure 3(c)).

As already said in the introduction, the proposed adaptive multiscale approach looks somewhat like the adaptive B-spline approach proposed earlier in [2]. However, the tools used are quite different; what matters most now is that one aims at achieving a localized description of the search domain.

3.3. Implementation considerations

Since the electrical parameter distribution to be estimated is most probably complex-valued (the real part represents the permittivity and the imaginary part is associated with the conductivity), following [6], the contrast function is taken as

$$\chi = \xi + i\eta, \quad (14)$$

where ξ and η are two real-valued auxiliary parameters. Then, the problem is transformed into the minimization of J depending on the two auxiliary vector parameters \mathbf{a}_ξ and \mathbf{a}_η (see [2] for more details). This formulation provides an efficient representation both for the real part and for the imaginary part of the contrast vector via suitable matrices \mathbf{B}_ξ and \mathbf{B}_η (i.e., the distribution of the spline functions at several scales) for both parts (see results in section 4.5).

In the two-scale relation (equation (8)) for stage S2, the expansion coefficients α_k are fixed to 1, i.e., the matrix \mathbf{B} is made of ‘normalized’ B-splines (see figures 3(b) and 3(c)). In fact, this has no influence since the expansion coefficient vector \mathbf{a} is also acting on each basis.

The initial guess of the algorithm has been fixed to zero. Of course it is possible to use a backpropagation technique to find an initial guess, yet the final results are observed to remain the same.

The initial scale of the used splines must be fixed also. It is not interesting to start with the coarsest scale, which means that one function represents the whole domain of search, as the initial coarse scale since in the refinement step this function will evidently be replaced by its finer-scale representation after useless calculations. That is why, in the numerical results section, the considered initial coarse scale is not made of one spline (at scale s_1) but it is made of its corresponding finer-scale representation (scale $s_1 - 1$).

One also had to fix the value of the threshold Th . During our experiments, it appears easy to choose this value since for a large band of values, very close results are obtained. In what follows and in general, the threshold value was fixed around 0.7.

4. Numerical results

4.1. Model parameters

The simulated experimental system (see figure 1) consists of N_s line sources regularly spaced between -5 and $+5$ m at $y_s = 0.5$ m, and of N_r sensors regularly spaced between -10 and $+10$ m at $y_r = 0.125$ m. The frequency of operation is $f = 300$ MHz. Half-space 1 is characterized by $\varepsilon_{r1} = 1$ and $\sigma_1 = 0$ S m⁻¹ and half-space 2 by $\varepsilon_{r2} = 2$ and $\sigma_2 = 0$ S m⁻¹.

The results displayed in the paper consist of maps of electrical contrasts within a search domain of size 1×1 m² and centred at $(x = 0.0$ m, $y = -0.5$ m) and of accompanying data.

In what follows, different configurations are investigated in order to appraise the proposed approach. Reconstructions obtained using the adaptive multiscale (AM) method and, for reference, a pixel-based conjugate-gradient (PB) algorithm [2] are shown.

4.2. Configuration I: single object with positive contrast

The first configuration consists of a square dielectric cylinder with permittivity $\varepsilon_{r\Omega_1} = 3$ (see figure 3). This object is 0.22 m sized and is centred at $(x = 0.25$ m, $y = -0.35$ m). The search domain is discretized into 33×33 cells. For this configuration, the number of receivers and sources is $N_r = 47$ and $N_s = 15$, respectively.

This simple one-object configuration is considered in order to exemplify the final distribution of the spline functions at several scales. For this configuration, the number of iterations for the minimization in step S1 is fixed to 5, and to 10 in step S2.2. The number of stages S2 is fixed to 10. Here, the global procedure is stopped after six stages S2 because the representation cannot be refined anymore (i.e., it is not ‘interesting’, due to our criterion, to replace any B-spline by its finer-scale representation).

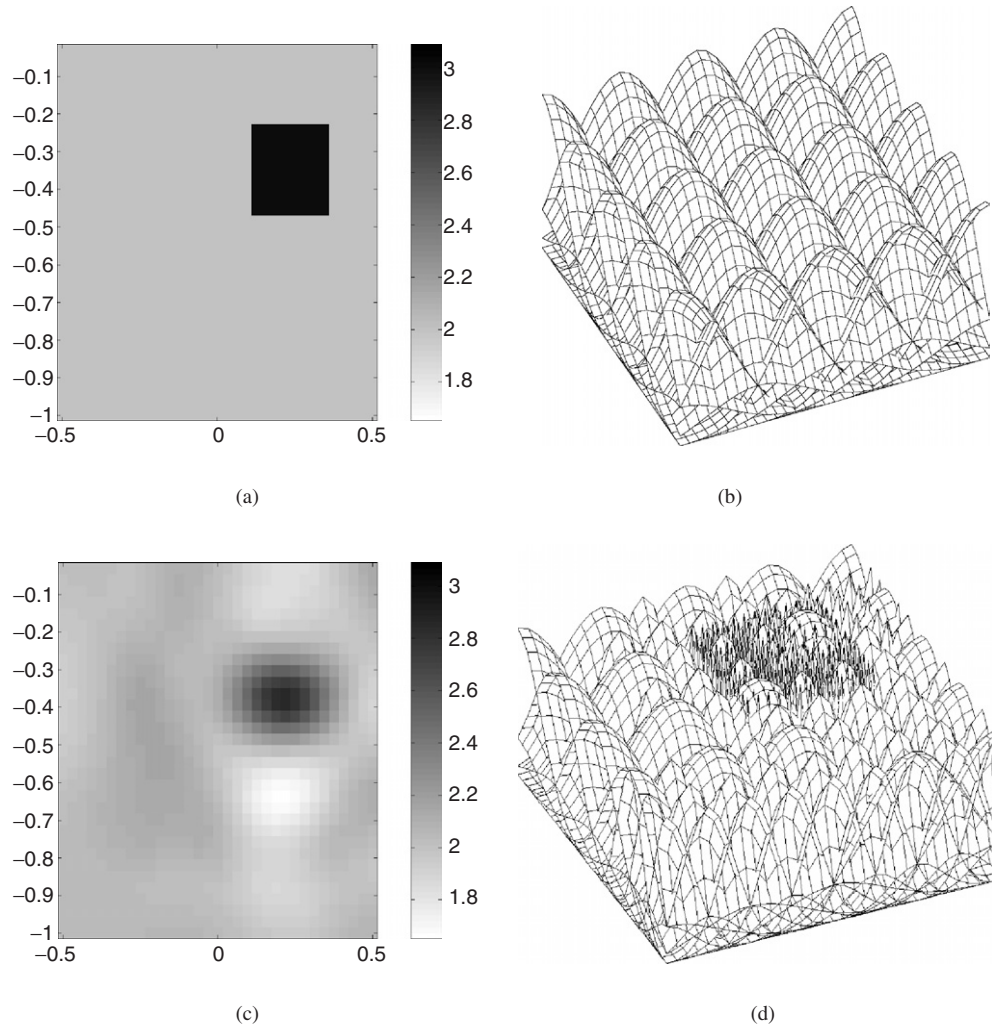


Figure 3. (a) Simulated configuration (I). (b) Initial coarse scale made of 25 B-splines (at scale 3). (c) Reconstruction reached by the adaptive multiscale method. (d) Final distribution made of 275 B-splines at several scales (scales: 3, 2, 1, 0).

Figure 3(a) shows the simulated object, figure 3(b) the spline distribution at the coarse scale made of 25 B-spline basis functions, figure 3(c) the retrieved map of the search domain, and figure 3(d) the corresponding distribution of B-splines made of 275 functions at several scales, that number comparing with the 1089 pixels of the discretized search domain.

Figure 4 illustrates the evolution of the global number of B-spline functions and of the number of B-splines for each scale at each iteration of the global procedure: the number of functions at stage S1 corresponds to iteration 0 and the number of functions at each stage S2 corresponds to iterations i ($i > 0$). Figure 5 shows the behaviour of the cost functional during the iterative procedure.

One can signal that the computational time is increased (here about 30%) with the AM method due to the refinement procedure. Future work should concentrate on the improvement of this particularly important stage.

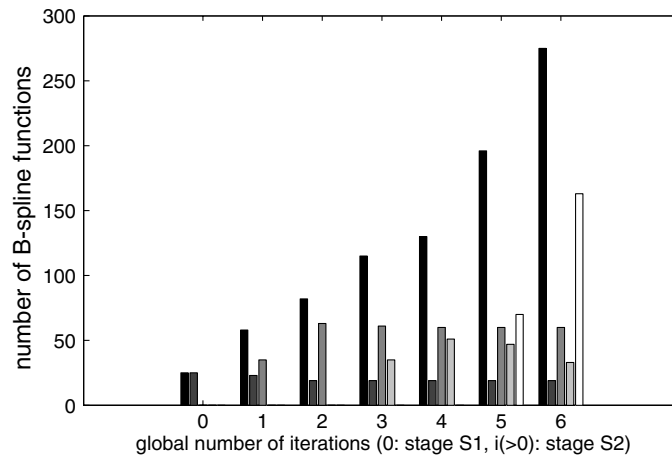


Figure 4. Evolution of the number of B-spline functions (configuration I). For each iteration, from left to right: global number of B-spline functions, number of functions at scale 3, 2, 1 and 0.

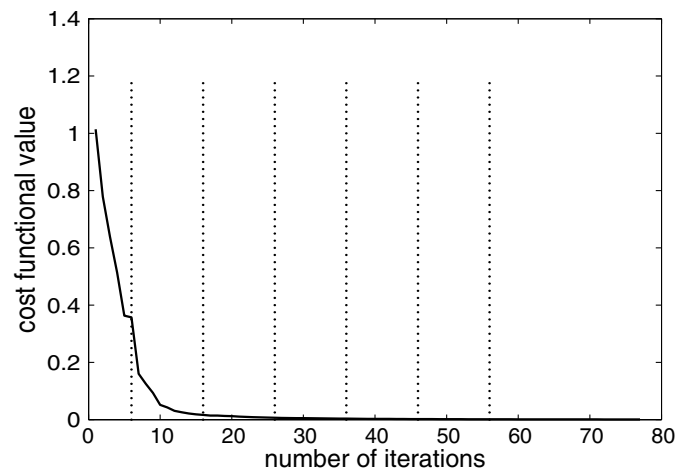


Figure 5. Evolution of the cost functional (equation (10)) during the procedure (configuration I). The vertical dashed lines highlight each beginning of a new stage S2.

Let us emphasize that, in step S2.1, it has been considered that the internal field is supposed unchanged. Figure 6 shows the results obtained in so doing (same as figure 3(c)) compared to those obtained when the internal field is updated during this step. The results are very close. The final number of spline functions in the case of the updating internal field was 305. The computational time was, of course, strongly increased. These results, and others one has obtained, appear to justify the ‘linearization’ affected in step S2.2.

4.3. Configuration II: two objects with positive contrasts

The second configuration is made of two dielectric cylinders (see figure 7). The lower one is square with side 0.25 m, centred at $(x = 0.2 \text{ m}, y = -0.8 \text{ m})$ and with permittivity $\varepsilon_{r\Omega_1} = 3$. The upper one is rectangular with sides 0.2 m (along x) and 0.25 m (along y),

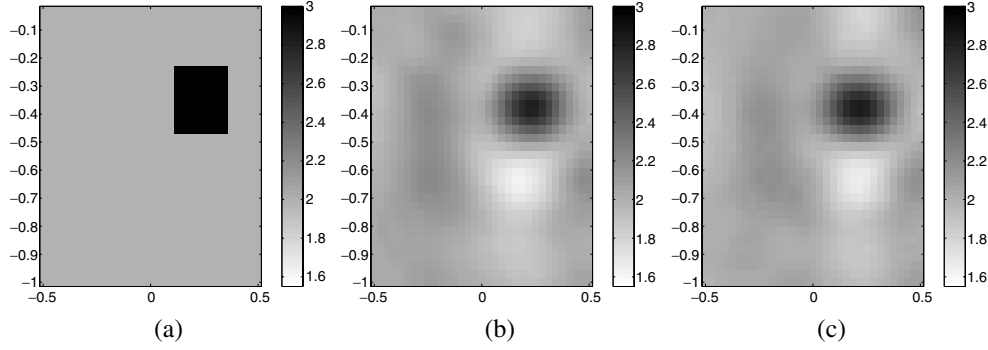


Figure 6. (a) Simulated configuration I. Reconstruction obtained using the adaptive multiscale method considering the total field (b) unchanged and (c) updated in step S2.2.

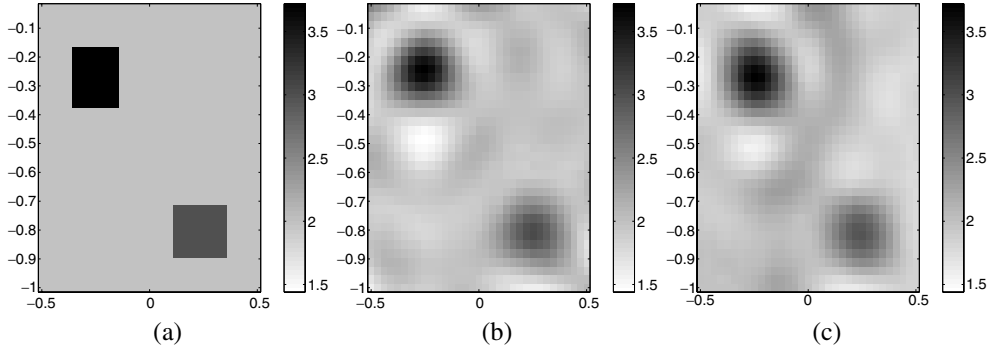


Figure 7. (a) Simulated configuration II. Reconstruction obtained using (b) the pixel-based method and (c) the adaptive multiscale approach.

Table 1. Values of several parameters for configuration II.

	Simulated object	PB method	AM approach
Iterations		65	$5 + 6 \times 10$
$\varepsilon_{r\Omega_1}$	3	3.02	2.99
$\varepsilon_{r\Omega_2}$	4	3.72	3.77
Number of elements	1089	1089	260

centred at $(x = -0.25 \text{ m}, y = -0.25 \text{ m})$, and with permittivity $\varepsilon_{r\Omega_2} = 4$. The search domain is discretized into 33×33 cells. For this configuration, the number of receivers and sources is $N_r = 47$ and $N_s = 15$, respectively.

The simulated configuration and the results obtained using the PB method and the AM approach are shown in figure 7. In this case, starting from the same coarse scale representation as for configuration I, the final estimate obtained with the AM approach is enhanced in comparison with the one yielded by the PB method (see the peak signal to noise ratio (*PSNR*) results in the next subsection). Table 1 gives the values of several parameters: the number of iterations in both inversion algorithms is specified first. Then, for the AM approach, one indicates the number of iterations in stage S1, the number of stages S2 and the number of iterations in step S2.2 (as follows, $S1 + S2 \times S2.2$). Note that the indicated number of iterations

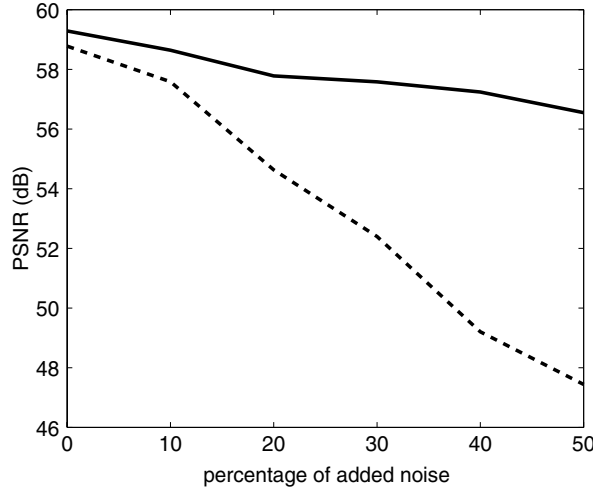


Figure 8. *PSNR* evolution for (- - -) the pixel-based method and for (—) the adaptive multiscale approach, depending on the percentage of noise added to the data, for configuration II.

in stage S2 corresponds to the number of iterations reached when the procedure is stopped (i.e., when it is not possible to refine the representation anymore). In table 1, one specifies also the maximum value of the permittivity of the reconstructed objects and the number of elements to be estimated (1681 pixels for the PB approach, to be compared to the 260 multiscale B-splines reached at the end of the AM procedure).

4.3.1. Noise effect. In order to exemplify the influence of noise on the reconstructions, the previous configuration (II) is considered with noise added to the scattered field as follows:

$$\mathbf{e}_{\text{noise}}^d = \mathbf{e}^d (1 + r \exp(i\phi)), \quad (15)$$

where r is the percentage of added noise and ϕ is a vector of random numbers in the range $[0, 2\pi]$.

To compare the reconstructions, depending on the noise level, the *PSNR*, commonly used in image processing, is introduced. It is defined for a b bits gray level by

$$PSNR = 10 \log \left(\frac{(2^b - 1)^2}{d} \right), \quad (16)$$

where d is the mean quadratic error given for a $[N_x \times N_y]$ image by

$$d = \frac{1}{N_x N_y} \sum_{i=0}^{N_x-1} \sum_{j=0}^{N_y-1} (I_0(i, j) - I_1(i, j))^2, \quad (17)$$

where I_0 is the true image (simulated object) and I_1 is the reconstructed image.

Figure 8 shows the evolution of the *PSNR* for the adaptive multiscale approach (black line) and the pixel-based approach (dashed line) for various noise levels, and figure 9 shows the reconstructions obtained for the scattered field with a noise level $r = 40\%$. From these results one can observe that addition of noise strongly affects the quality of the reconstructions (the *PSNR* decreases with increasing added noise) obtained with the PB method. This effect is much smaller with the proposed AM scheme. Hence, by controlling the degree of freedom of the inversion procedure one obtains a degree of robustness that does not require the use of

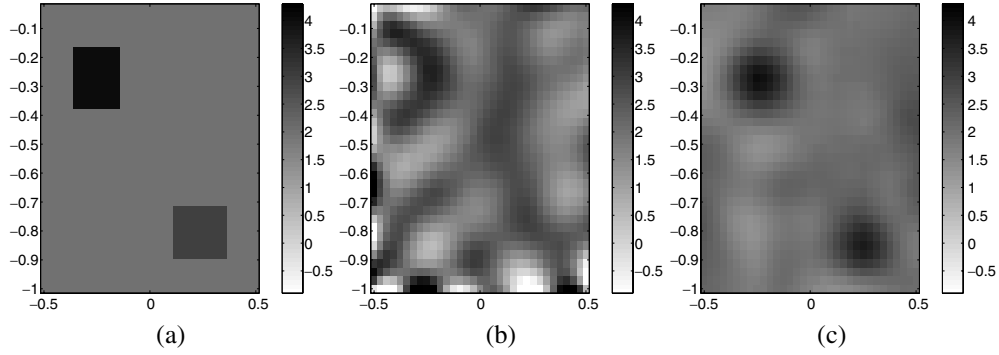


Figure 9. (a) Simulated configuration II. Reconstruction obtained using (b) the pixel-based algorithm and (c) the adaptive multiscale method with 40% noise.

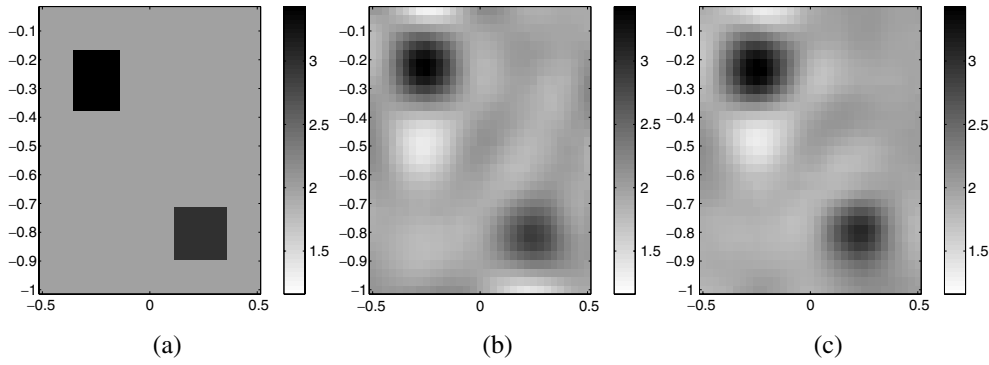


Figure 10. (a) Simulated configuration II with limited data. Reconstruction obtained using (b) the pixel-based algorithm and (c) the adaptive multiscale method.

Table 2. Parameter values for the configuration II with limited data.

	Simulated object	PB method	AM approach
Iterations		95	$5 + 6 \times 15$
$\varepsilon_{r\Omega_1}$	3	2.89	3.07
$\varepsilon_{r\Omega_2}$	4	3.43	3.48
Number of elements	1089	1089	198
<i>PSNR</i> (dB)		57.38	57.62

an explicit regularization functional. As indicated in section 1, at coarse scales, this spline representation enforces smoothness conditions.

4.3.2. Limited data. In this part, our approach is tested against limited data, i.e. the number of receivers and sources is reduced to $N_r = 15$ and $N_s = 5$, respectively. As it is a more challenging problem, due to the small number of available data, the number of iterations in stage S2.2 had to be increased.

The results are shown in figure 10. Table 2 gives, as in table 1, the values of parameters of interest. In addition, one specifies the *PSNR*-value which ‘quantifies’ the quality of the AM

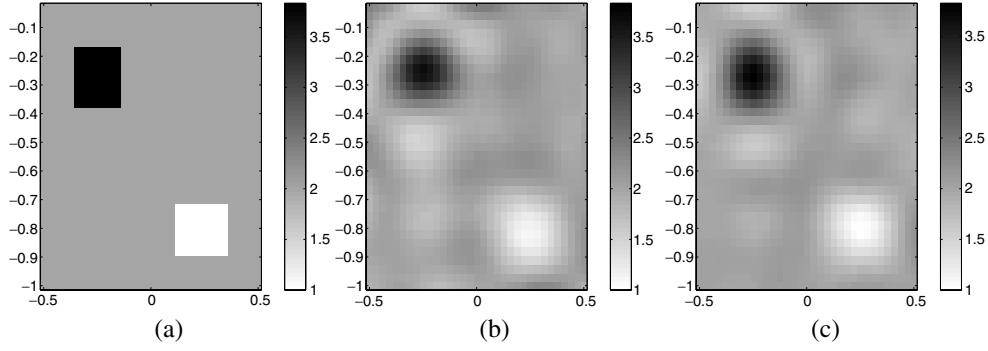


Figure 11. (a) Simulated configuration III. Reconstruction obtained using (b) the pixel-based algorithm and (c) the adaptive multiscale method.

Table 3. Same as table 2 for configuration III.

	Simulated object	PB method	AM approach
Iterations		65	$5 + 6 \times 10$
$\varepsilon_{r\Omega_1}$	1	1.10	0.99
$\varepsilon_{r\Omega_2}$	4	3.67	3.83
Number of elements	1089	1089	207
PSNR (dB)		58.78	59.98

reconstruction in comparison with the PB reconstruction. In this case both reconstructions are very close. The deeper object might be retrieved a little better with the AM algorithm.

4.4. Configuration III: two objects with positive or negative contrasts

In this configuration, there are two dielectric cylinders with permittivity $\varepsilon_{r\Omega_1} = 1$ and $\varepsilon_{r\Omega_2} = 4$ (see figure 11). The shallower one (Ω_2) is rectangular with sides 0.2 m (along x) and 0.25 m (along y) and is centred at $(x = -0.25 \text{ m}, y = -0.25 \text{ m})$. The deeper one (Ω_1) is square with side 0.25 m and is centred at $(x = 0.2 \text{ m}, y = -0.8 \text{ m})$. The search domain is discretized into 33×33 cells. For this configuration, the number of receivers and sources is $N_r = 47$ and $N_s = 15$, respectively.

Figure 11 shows the simulated configuration and the reconstructions obtained with the PB method and the AM approach. Both solutions are very close. Table 3 shows the different parameter values. Starting from a distribution of 25 basis functions, the final distribution is made of 207 basis functions (at several scales). Again, this should be compared with the 1089 elements to be estimated in the pixel-based approach.

4.5. Configuration IV: two objects, one conductive, one dielectric

This configuration involves two cylinders: a dielectric one with permittivity $\varepsilon_{r\Omega} = 3$, and a metallic one with conductivity $\sigma_{\Omega} = 1 \text{ S m}^{-1}$ (see figures 12(a) and 12(d)). The dielectric object is square with sides 0.17 m and is centred at $(x = -0.25 \text{ m}, y = -0.32 \text{ m})$. The metallic one is rectangular with sides 0.35 m (along x) and 0.25 m (along y) and is centred at $(x = 0.2 \text{ m}, y = -0.75 \text{ m})$. The search domain is discretized into 41×41 cells. For this configuration, the number of receivers and sources is $N_r = 47$ and $N_s = 15$, respectively.

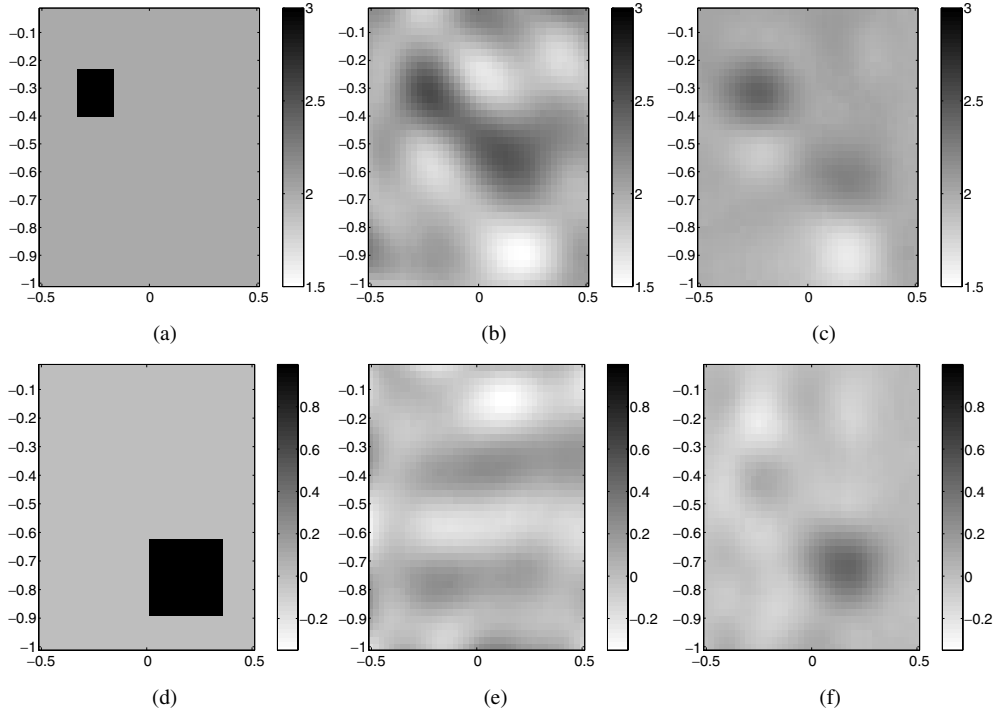


Figure 12. (a) Real and (d) imaginary parts of the simulated configuration IV. (b) Real and (e) imaginary parts of the contrast solution obtained using the pixel-based algorithm. (c) Real and (f) imaginary parts of the contrast solution obtained using the adaptive multiscale method.

Table 4. Values of several parameters for the configuration IV.

	Simulated object	PB method	AM approach
Iterations		65	$5 + 5 \times 12$
$\varepsilon_r \Omega$	3	2.56	2.43
σ_Ω ($S m^{-1}$)	1	0.27	0.47
Number of elements for the real part	1681	1681	269
Number of elements for the imaginary part	1681	1681	218
<i>PSNR</i> for the real part (dB)		61.58	64.36
<i>PSNR</i> for the imaginary part (dB)		58.44	60.57

Figure 12 shows the results obtained for this challenging problem and table 4 gives the corresponding parameter values. Overall, though the results are not very good, and real and imaginary parts tend to get mixed together, one should notice that the two objects can be detected with the AM scheme and not with the PB one. Moreover, for the PB method, the value of σ in table 4, has no meaning since in effect the conductive object is not detected.

5. Conclusion

In this contribution an adaptive multiscale inversion scheme based on the use of spline pyramids has been investigated. This coarse-to-fine based procedure takes advantage of the smoothness

conditions imposed by the spline representation, which tends to regularize the problem. It is an adaptive multiscale scheme since one automatically introduces finer-scale representations within interesting areas (i.e., near and within objects in the search domain) so that the final estimate is made of spline functions at several scales. The proposed approach leads to a reduction in the number of unknowns in the problem, improves the robustness of the inversion procedure and could enhance the final localization and characterization of buried objects. In the results shown, the reconstructions obtained with the adaptive multiscale approach are never worse than the reconstruction with the pixel-based approach. But an enhancement is particularly notable for challenging problems such as noisy data and the simultaneous retrieval of two metallic and dielectric objects.

A number of algorithmic issues remain, even in the rather ideal 2-D scalar case investigated. In particular, it would be useful to develop a clever (and computationally cheap) method to replace fine-scale B-splines by coarse-scale ones if needed. Also, in the refinement step, a 'one-by-one' procedure was considered. Through numerical simulations, this approach has been shown to be useful even though it is not a global procedure wherein all combinations of refinement are tested. A brute-force approach to this combinatorial problem is certainly intractable, however improvements (using e.g. more divide-and-conquer methods or perhaps branch-and-bound ideas) over the essentially greedy method developed in this paper are certainly an area of interest for future work.

References

- [1] Baussard A and Miller E L 2003 Detection and characterization of buried objects using an adaptive B-spline scheme *IEEE Conf. on Geoscience and Remote Sensing (IGARSS) (Toulouse)* vol 6, pp 3833–5
- [2] Baussard A, Miller E L and Prémel D 2004 Adaptive B-spline scheme for solving an inverse scattering problem *Inverse Problems* **20** 347–65
- [3] Chew W C and Wang Y M 1990 Reconstruction of two-dimensional permittivity distribution using the distorted Born iterative method *IEEE Trans. Medical Imaging* **9** 218–25
- [4] Couvreur C and Bresler Y 2000 On the optimality of the backward greedy algorithm for the subset selection problem *SIAM J. Matrix Anal. Appl.* **21** 797–808
- [5] Dierckx P 1993 *Curve and Surface Fitting with Splines* (New York: Oxford University Press)
- [6] Dourthe C, Pichot C, Dauvignac J Y, Blanc-Féraud L and Barlaud M 2000 Regularized bi-conjugate gradient algorithm for tomographic reconstruction of buried objects *IEICE Trans. Electron.* (Special issue on Problems on Random Scattering and Electromagnetic Wave sensing) **E83-C** 1858–63
- [7] Duchêne B and Tabbara W 1984 Characterization of a buried cylindrical object from its scattered field *IEEE Trans. Sonics Ultrasonics* **31** 658–63
- [8] Harrington F R 1968 *Field Computation by Moment Methods* (New York: Macmillan)
- [9] Joachimowicz N, Pichot C and Hugonin J P 1991 Inverse scattering: an iterative numerical method for electromagnetic imaging *IEEE Trans. Antennas Propag.* **39** 1742–51
- [10] Kleinman R E and Van den Berg P M 1992 A modified gradient method for two dimensional problems in tomography *J. Comput. Appl. Math.* **42** 17–35
- [11] Miller E L, Yavuz I, Nicolaidis L and Mandelis A 2000 An adaptive multiscale inverse scattering approach to photothermal depth profilometry *Circuits Systems Signal Process.* (Special issue on Advanced signal/image reconstruction) **19** 339–63
- [12] Strang G and Nguyen T 1996 *Wavelet and Filter Banks* (Wellesley, MA: Wellesley-Cambridge Press)
- [13] Thévenaz P, Rittmann U E and Unser M 1998 A pyramidal approach to subpixel registration based on intensity *IEEE Trans. Image Process.* **7** 27–41
- [14] Unser M 1999 Splines: a perfect fit for signal and image processing *IEEE Signal Process. Mag.* **16** 22–38
- [15] Van den Berg P M and Kleinman R E 1997 A contrast source inversion method *Inverse Problems* **13** 1607–20